THE UNIVERSITY of EDINBURGH

Edinburgh Research Explorer

In the Quest of a Parametric Relation Between Ice Sheet Model Inferred Weertman Sliding-Law Parameter and Airborne Radar-Derived Basal Reflectivity Underneath Thwaites Glacier, Antarctica

In the Quest of a Parametric Relation Between Ice Sheet Model Inferred Weertman's Sliding-Law Parameter and Airborne Radar-Derived Basal Reflectivity Underneath Thwaites Glacier, Antarctica

Indrani Das[1] , **Mathieu Morlighem[2]** , **Jowan Barnes[3]** , **G. Hilmar Gudmundsson[3]** , **Daniel Goldberg[4]** , **and Thiago Dias dos Santos[5]**

[1]Lamont-Doherty Earth Observatory, Columbia University, Palisades, NY, USA, [2]Dartmouth College, Hanover, NH, USA, [3]Northumbria University, Newcastle, UK, [4]University of Edinburgh, Scotland, UK, [5]University of São Paulo, São Paulo, Brazil

Abstract Numerical ice sheet models use sliding laws to connect basal shear stress and ice velocity to simulate ice sliding. A sliding-law parameter β^2 is used to control Weertman's sliding law in numerical ice sheet models. Basal reflectivity derived from ice-penetrating radar also provides information about frozen or thawed conditions underneath glaciers. To assess whether basal reflectivity can be used to constrain β^2, we carry out statistical experiments between two recently published datasets: β^2 inferred from three numerical ice sheet models (ISSM, Úa and STREAMICE) and airborne radar-derived relative basal reflectivity from the AGASEA-BBAS mission over Thwaites Glacier (TG). Our results show no robust correlation between the β^2–relative reflectivity pair. Pearson's correlation coefficient, a test of linearity, ranges from -0.26 to -0.38. Spearman's correlation coefficient, which does not require a linear assumption, is also modest (~-0.35). We conclude that β^2 and relative basal reflectivity underneath TG do not infer similar basal conditions.

Plain Language Summary Ice sheet models use equations called sliding laws to simulate how fast or slow ice can flow over the bed of a glacier. One such sliding law is Weertman's sliding law, which is widely used by numerical ice sheet models. A parameter called β^2 is used in Weertman's sliding law to match the observed velocity. Another parameter called basal reflectivity, derived from airborne ice penetrating radar data, is widely used to identify whether the bed underneath a glacier is frozen or thawed. Frozen or thawed conditions impact how fast a glacier can slide over its bed. Here, we try to find statistical correlations between β^2 and basal reflectivity over Thwaites Glacier (TG), West Antarctica. Our results show that the correlation values are not robust, which suggests that β^2 and basal reflectivity do not identify similar conditions at the bed underneath TG.

1. Introduction

Thwaites Glacier (TG) is uniquely situated in the warmer Amundsen Sea Sector, on a largely retrograde bed slope located below sea level. It is hypothesized that its rapid retreat may cause unbounded drainage of ice triggered by instabilities that could destabilize the West Antarctic Ice Sheet (Joughin et al., 2014; Scambos et al., 2017). Satellite observations indicate an acceleration of the glacier on its bed, likely initiated by the progressive loss and severe damage of its floating extensions and the large retreat rates experienced by some parts of its grounding line (Milillo et al., 2019; Rignot et al., 2013). Basal processes are critically responsible for faster retreat of the ice sheets and are notoriously difficult to observe and parameterize in models, particularly for a large and rapidly-evolving glacier like TG. Model intercomparison experiments highlight the lack of consensus on the representation of physical processes as a major cause of the large variations in sea level rise projections (e.g., Cornford et al., 2020; Goelzer et al., 2020; Seroussi et al., 2020).

Numerical ice sheet models use basal sliding laws that connect basal shear stress with ice velocity for projections of an ice sheet's contribution to sea level. A number of sliding laws have been proposed in literature. These include Weertman's sliding law that relates to hard non-deformable beds as well as those that incorporate Coulomb's friction law to simulate faster flow processes and transport of sediments (Iverson et al., 1998; Schoof, 2006; Tsai et al., 2015, 2017; Zoet & Iverson, 2020). The choice of the sliding law in numerical ice sheet models is important

Methodology: Indrani Das, Mathieu Morlighem, Jowan Barnes, G. Hilmar Gudmundsson, Daniel Goldberg, Thiago Dias dos Santos
Project Administration: Mathieu Morlighem, G. Hilmar Gudmundsson
Visualization: Indrani Das
Writing – original draft: Indrani Das, Mathieu Morlighem
Writing – review & editing: Mathieu Morlighem, Jowan Barnes, G. Hilmar Gudmundsson, Daniel Goldberg, Thiago Dias dos Santos

because it compounds to the large uncertainty in projections of sea level rise (De Rydt et al., 2021; Helanow et al., 2022; Joughin et al., 2019; Nias et al., 2019; Nowicki et al., 2013).

Catchment-wide observations of bed conditions are necessary to constrain basal conditions in ice sheet models. Localized seismic studies on TG show variable bed characters with regions of soft, deforming till as well as pooled ground water (Muto et al., 2019). Sedimentary deposits beneath the main trunk and tributaries of the neighboring Pine Island Glacier are inferred from seismic reflection studies (Brisbourne et al., 2017). High-resolution radar data (DELORES monopulse radars) collected over ~1,500 km² over Pine Island Glacier's tongue also demonstrate contrasting topography across the ice-bed interface that influences ice flow (Bingham et al., 2017). Basal reflectivity derived from airborne ice-penetrating radar data has been used to interpret basal conditions underneath TG, in particular the presence of liquid water, and subglacial hydrology (Chu et al., 2021; Peters et al., 2005; Schroeder et al., 2016). In this work, we explore whether the ice sheet model inferred basal sliding-law parameter β^2 used to constrain Weertman's sliding law (Figures 1a–1c; from Barnes et al., 2021) and relative basal reflectivity (Figures 1d–1e; from Chu et al., 2021) correlate well and identify similar conditions at the bed underneath Thwaites (Figure 1f).

2. Data Sets Used for the Correlation Experiments

2.1. Ice Sheet Model Inferred Basal Sliding-Law Parameter β^2

We use the basal sliding-law parameter β^2 from Barnes et al. (2021). β^2 used here is inferred from three ice sheet models: Ice-sheet and Sea-level System Model (ISSM; Larour et al., 2012), Úa (Gudmundsson, 2020) and the STREAMICE module of MITgcm (Goldberg & Heimbach, 2013). β^2 is inferred from velocity inversions using an adjoint framework (MacAyeal, 1993) and is also referred to as the basal friction or roughness coefficient. All three models employ Weertman's sliding law (Weertman, 1957) parameterized in Equations 1–3:

$$\text{ISSM}: \tau_b = \beta^2 \|v_b\|^{\frac{1}{m}-1} v_b \tag{1}$$

$$\text{Úa}: \tau_b = (C + C_0)^{-\frac{1}{m}} \left(\|v_b\|^2 + v_0{}^2 \right)^{(1-m)/2m} v_b \tag{2}$$

$$\text{STREAMICE}: \tau_b = \beta^2 \left(\|v_b\|^2 + v_0{}^2 \right)^{(1-m)/2m} v_b \tag{3}$$

where τ_b is the basal shear stress and v_b is the basal velocity. β is squared to avoid negative values and includes the model regularization terms C_0 and v_0. The sliding law exponent m is held constant at $m = 3$ in the inversions. Úa inverts for basal sliding coefficient C which has been converted to β^2 using $C = \left(\beta^2 \right)^{-m}$ to align with ISSM and STREAMICE.

2.2. Airborne Radar-Derived Relative Basal Reflectivity

We use the published relative basal reflectivity values from Chu et al. (2021) for statistical correlations with β^2. For ease of reading, we briefly describe their methodology here; for more details, the readers are referred to Chu et al. (2021). They use an adaptive empirical slope-based attenuation correction technique for calculating basal reflectivity (Schroeder et al., 2016). In this technique, the radar attenuation through ice is calculated within an initial radius of 20 km which can be adaptively incremented to a maximum radius of 500 km until a fixed set of criteria is met (Chu et al., 2021). The reflectivity values are relative because the mean reflectivity value has been subtracted from the total reflectivity values. The relative reflectivity values are also corrected for basal roughness and geometric spreading losses (Chu et al., 2021; Jordan et al., 2017; Matsuoka et al., 2010). Higher relative reflectivity values (≥10–20 dB) are used to identify subglacial water (Chu et al., 2016; Peters et al., 2005) and intrusion of sea water into the grounding zone (Parizek et al., 2013). Other studies have used the specularity content of radar data to investigate subglacial drainage geometry (e.g., Schroeder et al., 2013).

3. Methods: Statistical Experiments to Compare Observed and Modeled Basal Parameters

3.1. Correlation Techniques

A parametric relation between β^2 and relative basal reflectivity has not been developed yet. As an initial guess, we assume that β^2 and relative basal reflectivity are linearly related. For a linear parametric relation, Pearson's corre-
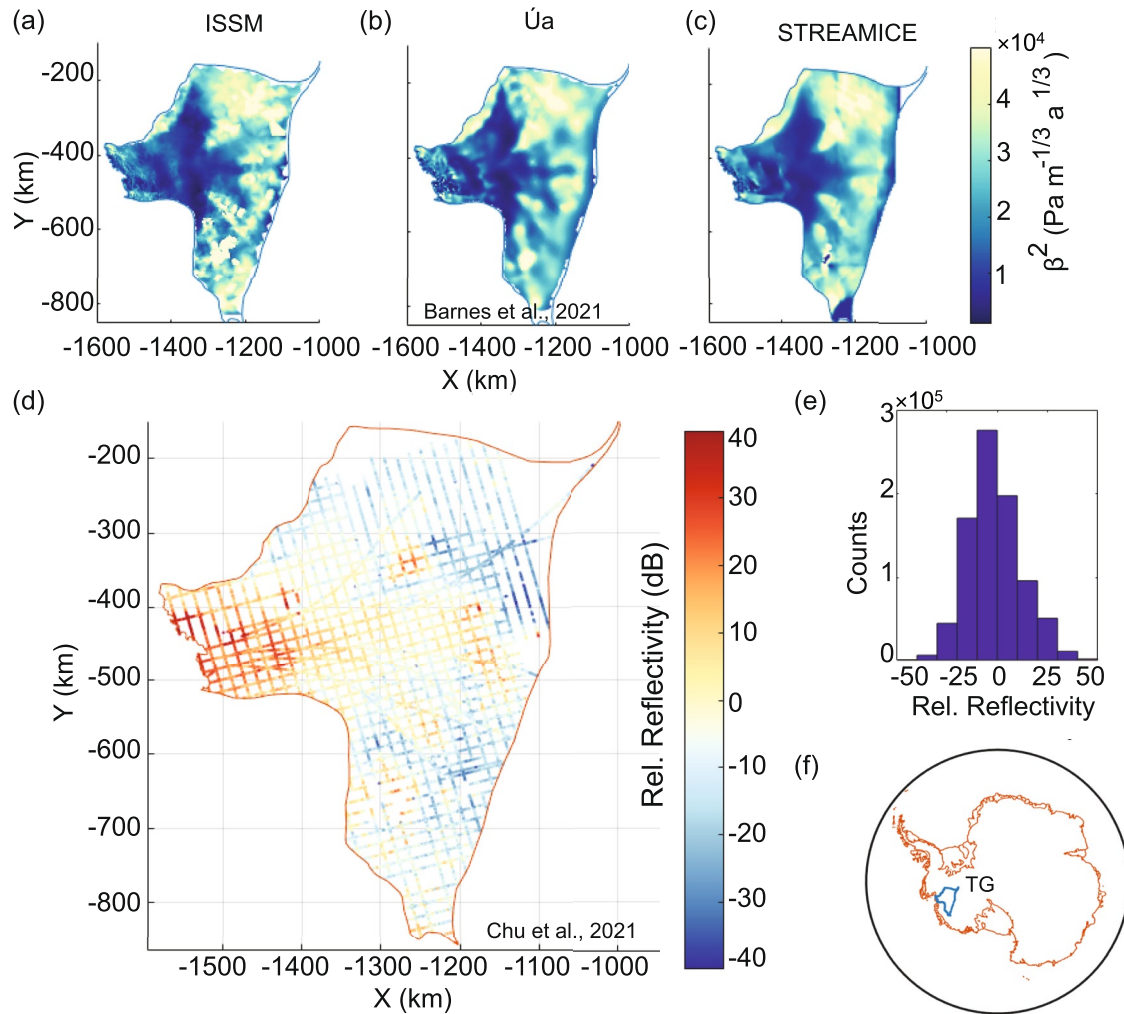
Figure 1. The modeled and observational datasets used for the correlation experiments: (a–c) β^2 inversions inferred from three ice sheet models (see Barnes et al., 2021); (d) AGASEA-BBAS radar-derived relative basal reflectivity from 2004 to 2005 (see Chu et al., 2021); (e) Histogram of the relative reflectivity data from (d); (f) Location of Thwaites Glacier (TG) in Antarctica.

lation coefficient is an appropriate technique to test the robustness and direction of association of the relation. Typically, a range of values is often proposed where a strong linear correlation is indicated by $\|r\| > 0.7$; and no correlation is indicated by $\|r\| < 0.3$. These ranges and the limits that define strong, moderate, and weak correlations are often arbitrary and should be judiciously interpreted (e.g., Schober et al., 2018). Researchers generally agree that very strong correlations approach a straight line (in either direction) with Pearson's correlation coefficient approaching $\|r\| > 0.9$ (Schober et al., 2018; Wackerly et al., 2008). However, a nonlinear relation between the variables will also output a low value of Pearson's correlation coefficient. If a nonlinear or curvilinear relation is suspected, Spearman's correlation coefficient is often calculated. In this work, we calculate both Pearson's and Spearman's coefficients for the β^2– relative reflectivity pair.

3.1.1. Pearson's Correlation Coefficient

The formula for Pearson's correlation coefficient (r) is

$$r = \frac{1}{n-1}\left[\sum_x \sum_y \frac{(x-\bar{x})(y-\bar{y})}{s_x s_y}\right] \tag{4}$$

where n is the number of pairs of data; $\overline{x}$ and $\overline{y}$ are the sample means of all the x and y values, respectively (here the β^2 and relative reflectivity values); and s_x and s_y are the sample standard deviations of the x and y values, respectively (Pearson, 1895).

3.1.2. Spearman's Correlation Coefficient

Spearman's rank correlation (also called Spearman's correlation or Spearman's ρ) does not require the relationship between the variables x and y to be linear. It can be used for non-normally distributed data, and is relatively robust to outliers (Equation 5; Spearman, 1904). Spearman's rank correlation is similar to Pearson's correlation except that it is calculated based on the ranks of the x and y variables rather than the actual values:

$$\rho = 1 - \frac{6 \sum d^2}{n(n^2 - 1)} \tag{5}$$

where d is the difference between the ranks of the two columns, and n is the sample size.

A value of 1 indicates that the two variables are not independent, and a value of zero indicates that the two variables are independent. Any value in-between conveys the degree of dependency between the two variables.

3.2. Preparing the Data Sets for the Correlation Experiments

We carry out the correlation experiments on two spatial scales: local scale and on a 15 km averaging box. For the first experiment, we interpolate β^2 directly on the original radar grid points and calculate Pearson's and Spearman's correlation coefficients. We call this experiment the "local-scale experiment." Because β^2 is inferred from numerical models with resolutions coarser than the radar data, the relative basal reflectivity and β^2 may not agree well on smaller spatial scales (Kyrke-Smith et al., 2017). Therefore, we also correlate the two variables on a larger spatial scale of 15 km. For this, we define boxes of 15-km widths around each radar coordinate and correlate the mean and the median values of the relative reflectivity with the mean of β^2 within this box. This is our "spatially-averaged experiment."

We also examine how higher values of m would impact the correlation results. We choose $m = 20$ which would represent a near-plastic bed (De Rydt et al., 2021; Gillet-Chaulet et al., 2016) in Equations 1–3, and carry out a simple scaling experiment described by Equations 6–8.

For this test, we note that wherever the ice sheet is grounded, the ice-sheet momentum balance used in the models dictates that basal drag is equal to the sum of the driving stress τ_d and membrane stress $M(v_b)$, that is,

$$\tau_d + M(v_b) = \tau_b(v_b) \tag{6}$$

Both membrane stress and basal drag have a dependence on velocity, which is made explicit here. However, if the functional dependence of basal drag on velocity were to be changed, the balance would still hold with the same velocity field, as long as basal drag were unchanged (Felikson et al., 2022; Brondex et al., 2019, 2017; Text S1 in Supporting Information S1). Thus, a higher value for m is considered as follows. We define a new basal drag coefficient β_{20}^2 through the relationships

$$\tau_b = \beta^2 v_b^{1/3}; \quad \tau_b = \beta_{20}^2 v_b^{1/20} \tag{7}$$

$$\beta_{20}^2 = \beta^2 \frac{v_b^{1/3}}{v_b^{1/20}} \tag{8}$$

where β^2 is the sliding law parameter corresponding to $m = 3$ and β_{20}^2 is the sliding law parameter corresponding to $m = 20$; and we carry out the correlations with β_{20}^2 derived from Equation 8.

4. Results

The spatial variation of β^2 and the corresponding relative reflectivity values over the Thwaites domain are shown in Figure 1. In general, β^2 values decrease from the upstream areas to the grounding zone. Conversely, the relative reflectivity values increase from upstream to the grounding zone. This is expected, because ice slides faster on

a thawed bed that offers lower resistance and generally has low β^2 and high relative reflectivity (e.g., box a1, Figure 2a). Initial assessment therefore suggests a negative correlation between the two parameters. However, both parameters have local variability. For example, pockets of higher relative reflectivity as high as the values near the grounding zone are observed in the upper elevations areas (box a2, Figure 2a). The corresponding β^2 values in this region are also high. The coherent nature of the relative reflectivity values suggests that these are likely not artifacts or errors in the data. Localized friction heating due to rougher bed could be responsible for the high relative reflectivity values in these areas.

The scatterplots of the β^2–relative reflectivity pair for the local-scale experiment are shown in Figures 2b–2d for the three ice sheet models. The warmer colors of the scatterplots indicate a higher density of points. Although the relative reflectivity values stretch from −50 to 50 dB in Figures 2b–2d, the number of points beyond −40 and +40 dB are insignificant (Figure 1e; Chu et al., 2021). The strength of the relation is specified by Pearson's and Spearman's correlation coefficients (Table 1). Pearson's coefficient ranges from −0.26 to −0.34 for the local-scale experiment for the three ice sheet models. The local-scale Spearman's coefficient is higher than Pearson's coefficient and ranges from −0.35 to −0.37 for the three models.

As we increase the size of the box to 15 km for the spatially-averaged experiment, Pearson's correlation coefficient shows a slight improvement and ranges from −0.29 to −0.37 for the three ice sheet models (Table 1). This range includes both the mean and the median filters used for averaging the relative reflectivity values in the 15 km boxes. As noted previously, the minimum radius for calculating the attenuation rates is 20 km (Chu et al., 2021). As the relative reflectivity values are sensitive to the choice of the attenuation rates, we anticipate that the relative reflectivity grid may be somewhat smoothed if one single attenuation rate is used for at least 20 km. In some difficult areas, this radius could be higher. We chose not to increase the averaging box to >15 km because it is not clear that would be physically justified for a fast-moving glacier such as Thwaites. We infer that as the correlation coefficients are lower than 0.4 (with a negative or downhill trend), a robust relation does not exist between the two variables. All three models perform similarly in all the experiments.

Our experiment with a higher value of m ($m = 20$) representing a near-plastic bed rheology (Equation 8) yields a Pearson's correlation coefficient of 0.12, 0.13, and 0.11 for ISSM, Úa and STREAMICE respectively (Table 1) indicating no correlation between the two parameters. In fact, our calculations indicate that any value of m between 3, which is usually used, and 20, which is an extreme case, does not improve the correlation (see Text S1 in Supporting Information S1).

The standard deviations of β^2 and relative reflectivity (Figures 3a–3d) are calculated within the 15 km boxes and demonstrate how variability in bed conditions are disparately captured by models and observations. For example, all three models show high standard deviations at one side of the grounding zone ($x \approx -1{,}500$ km and $y \approx -500$ km) with low relative reflectivity variations. In contrast, the high variability in relative reflectivity values in the region around $x \approx -1{,}300$ km and $y \approx -650$ km are not equally identified by the three models.

5. Discussions

In this work, we compare model-inferred β^2 with relative basal reflectivity and observe no robust correlations. Based on limited observations of the bed underneath Thwaites and Pine Island glaciers (Bingham et al., 2017; Brisbourne et al., 2017; Muto et al., 2019), we know that the bed conditions underneath both of these glaciers are variable, with regions of soft, deformable till and scattered presence of water. Is it possible that incorporating effective pressure via Coulomb friction would have correlated better with the relative basal reflectivity? Would the correlations have been different for a slower flowing glacier? These questions highlight the unknown bed conditions over large/catchment scales that impact ice flow. With improved geophysical observations of the bed along larger spatial domains, these avenues can be explored.

The choice of the exponent m could also influence the inferred spatial distribution of β^2. On the Pine Island Glacier catchment, the value of m has been inferred to be ~20, closely aligned with a near-plastic bed rheology (De Rydt et al., 2021; Gillet-Chaulet et al., 2016). However, our simple experiment with $m = 20$ does not yield a better Pearson's correlation coefficient over TG. The low correlation values achieved with $m = 3, 7, 10$, and 20 (Text S1, Supporting Information S1) indicate that any other value of m between 3 and 20 in Weertman's sliding law is unlikely to improve the correlation of β^2 with the relative basal reflectivity used in this analysis.
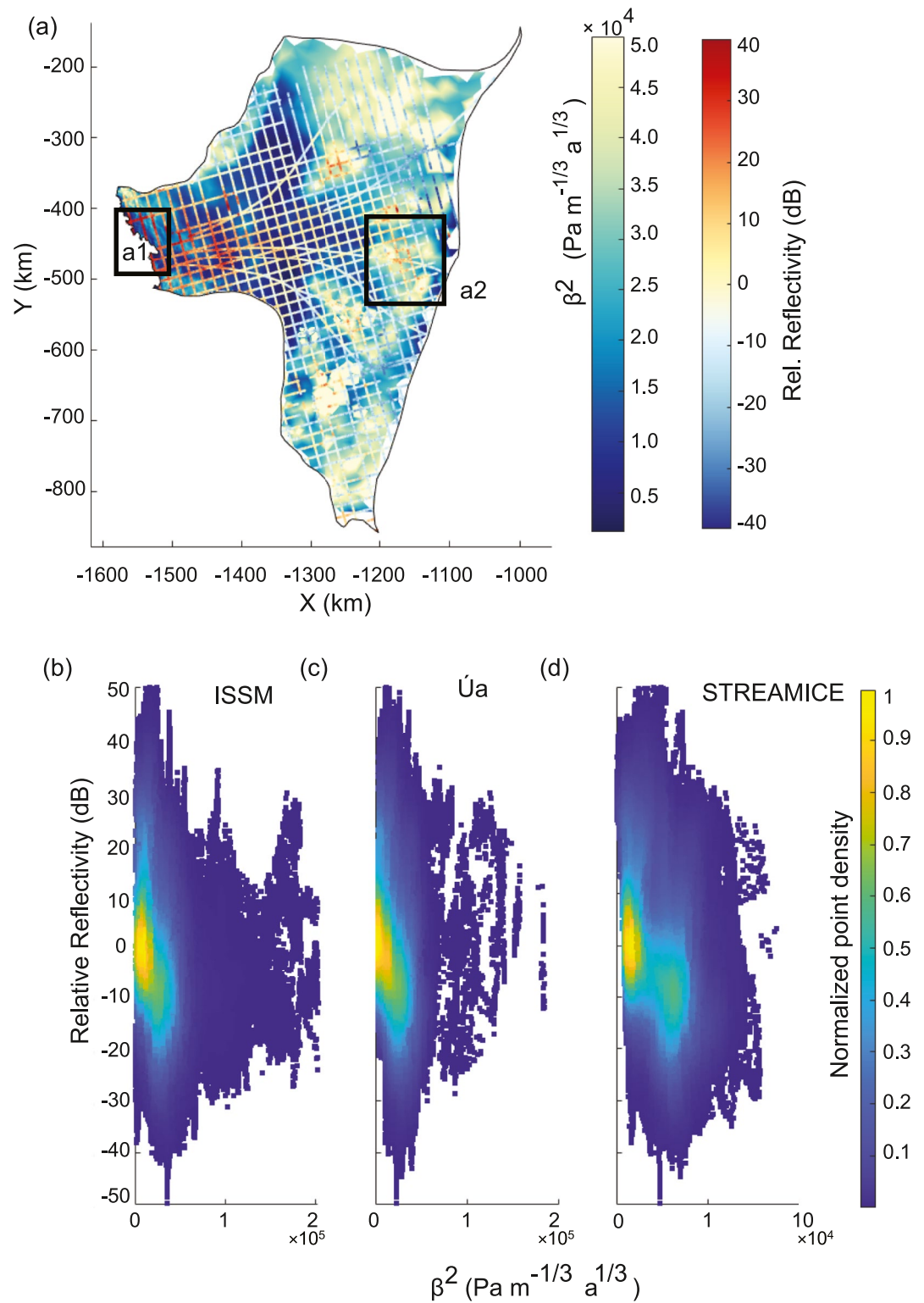
Figure 2. Correlation experiments: (a) Spatial variation of sliding-law parameter β^2 and relative basal reflectivity; a1 shows regions where relative reflectivity is high with generally low β^2, and a2 is a region where a localized pocket of high relative reflectivity is associated with high β^2; (b–d) Scatterplots of β^2 with relative basal reflectivity for the local-scale experiment (b) ISSM; (c) Úa; (d) STREAMICE (note the shorter x-axis scale for STREAMICE due its smaller spread of β^2).

Table 1
Correlation Values Between β^2 and Relative Basal Reflectivity

| Ice sheet model	Pearson's correlation coefficient (local-scale) $m = 3$	Spatially-averaged 15 km mean/median filtered correlation experiment (Pearson's) $m = 3$	Spearman's correlation coefficient (local-scale) $m = 3$	Pearson's correlation coefficient (local-scale) $m = 20$
ISSM	−0.26	−0.3/−0.29	−0.35	0.12
Úa	−0.28	−0.32/−0.31	−0.34	0.13
STREAMICE	−0.34	−0.38/−0.37	−0.37	0.11

Most sliding laws currently used follow Weertman-like behavior throughout most of the domain, with the Coulomb friction component only active in a narrow band near the grounding line. Therefore, it is probable that any catchment-scale correlation would be similar to what we have calculated in this paper.

The physical interpretation of the relative basal reflectivity values is also non-unique as *in-situ* measurements of basal conditions are very rare and comparisons cannot be readily made. Multiple processes—including subglacial water, frictional heat dissipation, water saturated sediments at the bed—can all result in high relative reflectivity values. In addition, measurement errors influence the values of the correlation coefficients (Saccenti et al., 2020; Spearman, 1904). With increased complexity of instruments and measured values, measurement errors are heterogenous, spatially variable and not independent. For example, including the uncertainties in relative
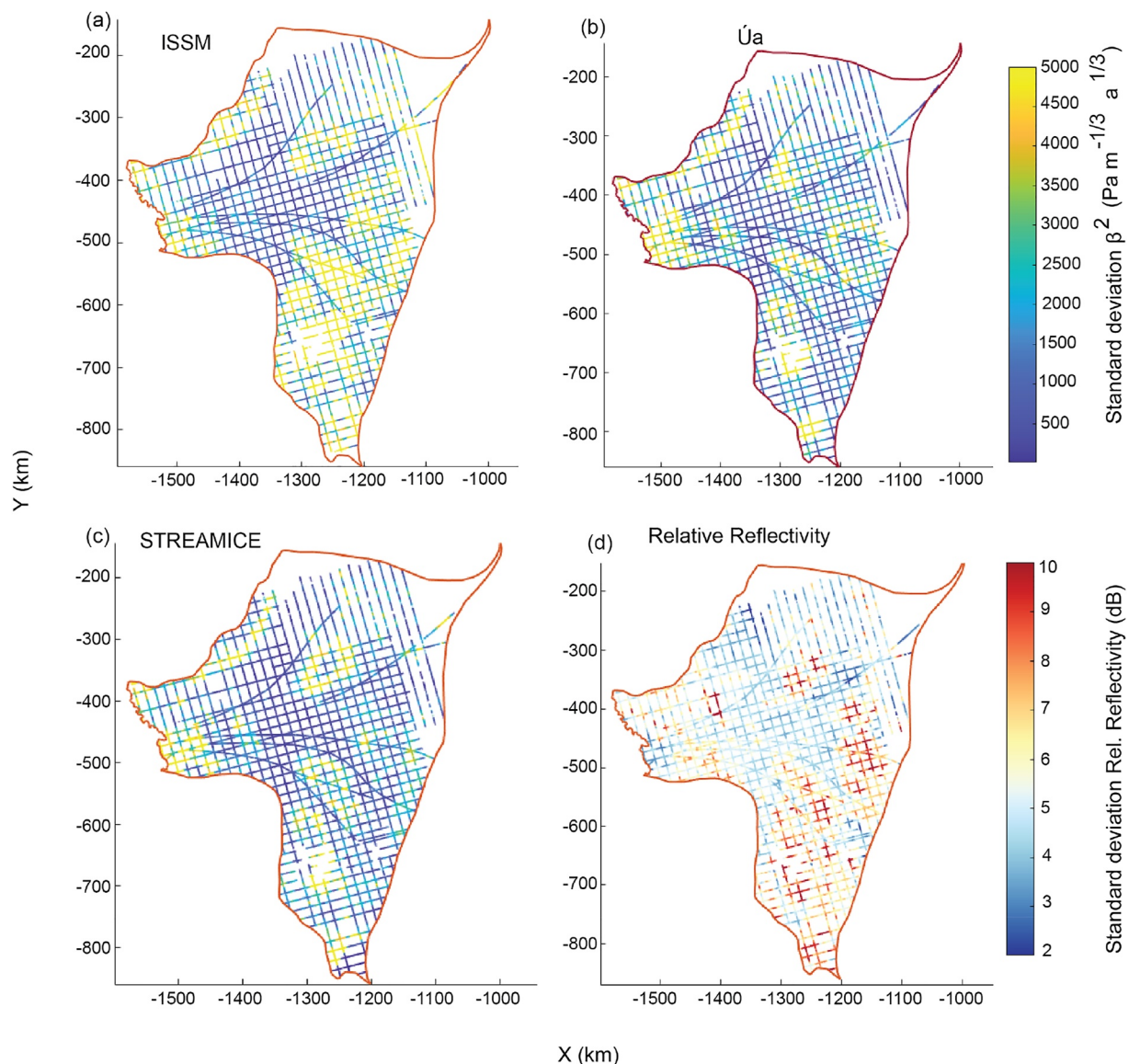
Figure 3. Standard deviations of β^2 and relative basal reflectivity within the 15 km box used in the correlation experiments (a) for ISSM (b) Úa (c) STREAMICE and (d) relative basal reflectivity.
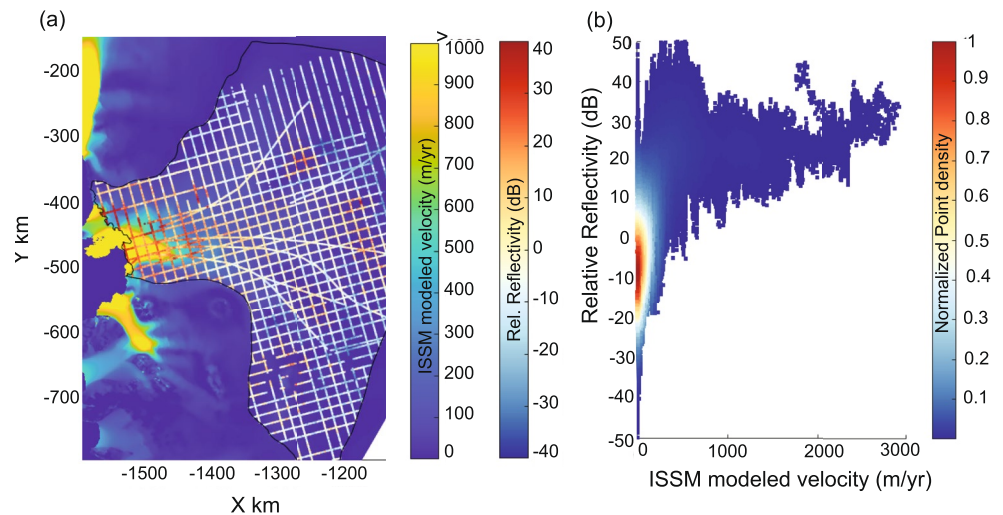
Figure 4. Comparison of relative basal reflectivity and modeled ice velocity: (a) Spatial variation of relative basal reflectivity and ISSM modeled ice velocity within the Thwaites domain; (b) Spread of ISSM modeled velocity and relative basal reflectivity.

basal reflectivity (Figure S1, Equations S1 and S2 in Text S2 of Supporting Information S1) provided by Chu et al. (2021) leads to an increase in ∥r∥, although very nominal, for all three ice sheet models, for both Pearson's and Spearman's methods (Table S1 in Text S2 of Supporting Information S1).

Our rationale for comparing the β^2–relative reflectivity pair is based on the assumption that they should be related via ice velocity. Our similar exercise of comparison of relative basal reflectivity with modeled ice velocity shows a better agreement with a Pearson's correlation coefficient of ~0.53 and a Spearman's coefficient of ~0.61 (Figures 4a and 4b). An initial assessment of the point cloud distribution of the velocity–relative reflectivity pair suggests the presence of a relation that is likely non-linear. Further work is needed to parameterize the velocity–relative reflectivity relation. It also needs to be assessed whether this point-cloud distribution is sensitive to the correction for attenuation rates through ice.

It should be noted that the correlations, although low, are uniformly negative for the β^2–relative reflectivity pair with $m = 3$, and positive for the relative reflectivity–velocity pair. At least this is physically valid. Exploring how relative basal reflectivity could be related to other processes such as intrusion of seawater near the grounding zone would be useful for interpreting complex basal conditions.

6. Conclusions

We compare inversions of β^2, known as the basal sliding-law parameter in Weertman's sliding law from three ice sheet models ISSM, Úa and STREAMICE with airborne radar-derived relative basal reflectivity from the AGASEA-BBAS mission. Pearson's correlation coefficient for the β^2–relative reflectivity pair ranges from −0.26 to −0.38 for all three ice sheet models. Spearman's correlation coefficient, often used if a curvilinear relationship is suspected, ranges from −0.34 to −0.37 for the three models. Based on the low values of the correlation coefficients, we conclude that a robust relationship does not exist between the β^2–relative reflectivity pair. The correlations do not improve even when a higher value of m is used. For relative basal reflectivity to provide independent constraints on the sliding law parameters in ice sheet models, robust correlations between these two quantities are needed. Our results suggest that β^2 and relative basal reflectivity do not infer similar conditions at the bed.

Data Availability Statement

The datasets from this study are available via USAP-DC website https://doi.org/10.15784/601658. The radar reflectivity data is available at https://doi.org/10.15784/601436 (see Chu et al., 2021).

References

Barnes, J. M., dos Santos, T., Goldberg, D., Gudmundsson, G. H., Morlighem, M., & De Rydt, J. (2021). The transferability of adjoint inversion products between different ice flow models. *The Cryosphere*, *15*(4), 1975–2000. https://doi.org/10.5194/tc-15-1975-2021

Bingham, R. G., Vaughan, D. G., King, E. C., Davies, D., Cornford, S. L., Smith, A. M., et al. (2017). Diverse landscapes beneath Pine Island Glacier influence ice flow. *Nature Communications*, *8*(1), 1618. https://doi.org/10.1038/s41467-017-01597-y

Brisbourne, A. M., Smith, A. M., Vaughan, D. G., King, E. C., Davies, D., Bingham, R. G., et al. (2017). Bed conditions of Pine Island Glacier, West Antarctica. *Journal of Geophysical Research: Earth Surface*, *122*(1), 419–433. https://doi.org/10.1002/2016JF004033

Brondex, J., Gagliardini, O., Gillet-Chaulet, F., & Durand, G. (2017). Sensitivity of grounding line dynamics to the choice of the friction law. *Journal of Glaciology*, *63*(241), 854–866. https://doi.org/10.1017/jog.2017.51

Brondex, J., Gillet-Chaulet, F., & Gagliardini, O. (2019). Sensitivity of centennial mass loss projections of the Amundsen basin to the friction law. *The Cryosphere*, *13*(1), 177–195. https://doi.org/10.5194/tc-13-177-2019

Chu, W., Schroeder, D. M., Seroussi, H., Creyts, T. T., Palmer, S. J., & Bell, R. E. (2016). Extensive winter subglacial water storage beneath the Greenland Ice Sheet. *Geophysical Research Letters*, *43*(24), 12484–12492. https://doi.org/10.1002/2016GL071538

Chu, W., Hilger, A. M., Culberg, R., Schroeder, D. M., Jordan, T. M., Seroussi, H., et al. (2021). Multisystem synthesis of radar sounding observations of the Amundsen Sea Sector from the 2004–2005 field season. *Journal of Geophysical Research: Earth Surface*, *126*(10), e2021JF006296. https://doi.org/10.1029/2021JF006296

Cornford, S. L., Seroussi, H., Asay-Davis, X. S., Gudmundsson, G. H., Arthern, R., Borstad, C., et al. (2020). Results of the third marine ice sheet model intercomparison project (MISMIP+). *The Cryosphere*, *14*(7), 2283–2301. https://doi.org/10.5194/tc-14-2283-2020

De Rydt, J., Reese, R., Paolo, F. S., & Gudmundsson, G. H. (2021). Drivers of Pine Island Glacier speed-up between 1996 and 2016. *The Cryosphere*, *15*(1), 113–132. https://doi.org/10.5194/tc-15-113-2021

Felikson, D., Nowicki, S., Nias, I., Csatho, B., Schenk, A., Croteau, M., & Loomis, B. (2022). Choice of observation type affects Bayesian calibration of ice sheet model projections. *EGUsphere*, 1–18. https://doi.org/10.5194/egusphere-2022-1213

Gillet-Chaulet, F., Durand, G., Gagliardini, O., Mosbeux, C., Mouginot, J., Rémy, F., & Ritz, C. (2016). Assimilation of surface velocities acquired between 1996 and 2010 to constrain the form of the basal friction law under Pine Island Glacier. *Geophysical Research Letters*, *43*(19), 10311–10321. https://doi.org/10.1002/2016GL069937

Goelzer, H., Nowicki, S., Payne, A., Larour, E., Seroussi, H., Lipscomb, W. H., et al. (2020). The future sea-level contribution of the Greenland ice sheet: A multi-model ensemble study of ISMIP6. *The Cryosphere*, *14*(9), 3071–3096. https://doi.org/10.5194/tc-14-3071-2020

Goldberg, D. N., & Heimbach, P. (2013). Parameter and state estimation with a time-dependent adjoint marine ice sheet model. *The Cryosphere*, *7*(6), 1659–1678. https://doi.org/10.5194/tc-7-1659-2013

Gudmundsson, G. H. (2020). GHilmarG/UaSource: Ua2019b (version v2019b). https://doi.org/10.5281/zenodo.3706623

Helanow, C., Iverson, N. R., Woodard, J. B., & Zoet, L. K. (2022). A slip law for hard-bedded glaciers derived from observed bed topography. *Science Advances*, *7*(20), eabe7798. https://doi.org/10.1126/sciadv.abe7798

Iverson, N. R., Hooyer, T. S., & Baker, R. W. (1998). Ring-shear studies of till deformation: Coulomb-plastic behavior and distributed strain in glacier beds. *Journal of Glaciology*, *44*(148), 634–642. https://doi.org/10.3189/S0022143000002136

Jordan, T. M., Cooper, M. A., Schroeder, D. M., Williams, C. N., Paden, J. D., Siegert, M. J., & Bamber, J. L. (2017). Self-affine subglacial roughness: Consequences for radar scattering and basal water discrimination in northern Greenland. *The Cryosphere*, *11*(3), 1247–1264. https://doi.org/10.5194/tc-11-1247-2017

Joughin, I., Smith, B. E., & Medley, B. (2014). Marine ice sheet collapse potentially under way for the Thwaites Glacier basin, West Antarctica. *Science*, *344*(6185), 735–738. https://doi.org/10.1126/science.1249055

Joughin, I., Smith, B. E., & Schoof, C. G. (2019). Regularized Coulomb friction laws for ice sheet sliding: Application to Pine Island Glacier, Antarctica. *Geophysical Research Letters*, *46*(9), 4764–4771. https://doi.org/10.1029/2019GL082526

Kyrke-Smith, T. M., Gudmundsson, G. H., & Farrell, P. E. (2017). Can seismic observations of bed conditions on ice streams help constrain parameters in ice flow models? *Journal of Geophysical Research: Earth Surface*, *122*(11), 2269–2282. https://doi.org/10.1002/2017JF004373

Larour, E., Seroussi, H., Morlighem, M., & Rignot, E. (2012). Continental scale, high order, high spatial resolution, ice sheet modeling using the Ice Sheet System Model (ISSM). *Journal of Geophysical Research*, *117*(F1), F01022. https://doi.org/10.1029/2011JF002140

MacAyeal, D. R. (1993). A tutorial on the use of control methods in ice-sheet modeling. *Journal of Glaciology*, *39*(131), 91–98. https://doi.org/10.3189/S0022143000015744

Matsuoka, K., Morse, D., & Raymond, C. F. (2010). Estimating englacial radar attenuation using depth profiles of the returned power, central West Antarctica. *Journal of Geophysical Research*, *115*(F2), F02012. https://doi.org/10.1029/2009JF001496

Milillo, P., Rignot, E., Rizzoli, P., Scheuchl, B., Mouginot, J., Bueso-Bello, J., & Prats-Iraola, P. (2019). Heterogeneous retreat and ice melt of Thwaites Glacier, West Antarctica. *Science Advances*, *5*(1). https://doi.org/10.1126/sciadv.aau3433

Muto, A., Anandakrishnan, S., Alley, R. B., Horgan, H. J., Parizek, B. R., Koellner, S., et al. (2019). Relating bed character and subglacial morphology using seismic data from Thwaites Glacier, West Antarctica. *Earth and Planetary Science Letters*, *507*, 199–206. https://doi.org/10.1016/j.epsl.2018.12.008

Nias, I. J., Cornford, S. L., Edwards, T. L., Gourmelen, N., & Payne, A. J. (2019). Assessing uncertainty in the dynamical ice response to ocean warming in the Amundsen Sea Embayment, West Antarctica. *Geophysical Research Letters*, *46*(20), 11253–11260. https://doi.org/10.1029/2019GL084941

Nowicki, S., Bindschadler, R. A., Abe-Ouchi, A., Aschwanden, A., Bueler, E., Choi, H., et al. (2013). Insights into spatial sensitivities of ice mass response to environmental change from the SeaRISE ice sheet modeling project I: Antarctica. *Journal of Geophysical Research: Earth Surface*, *118*(2), 1002–1024. https://doi.org/10.1002/jgrf.20081

Parizek, B. R., Christianson, K., Anandakrishnan, S., Alley, R. B., Walker, R. T., Edwards, R. A., et al. (2013). Dynamic (in)stability of Thwaites Glacier, West Antarctica. *Journal of Geophysical Research: Earth Surface*, *118*(2), 638–655. https://doi.org/10.1002/jgrf.20044

Pearson, K. (1895). Note on regression and inheritance in the case of two parents. *Proceedings of the Royal Society of London*, *58*, 240–242. Retrieved from http://www.jstor.org/stable/115794

Peters, M. E., Blankenship, D. D., & Morse, D. L. (2005). Analysis techniques for coherent airborne radar sounding: Application to West Antarctic ice streams. *Journal of Geophysical Research*, *110*(B6), B06303. https://doi.org/10.1029/2004jb003222

Rignot, E., Jacobs, S., Mouginot, J., & Scheuchl, B. (2013). Ice-shelf melting around Antarctica. *Science*, *341*(6143), 266–270. https://doi.org/10.1126/science.1235798

Saccenti, E., Hendriks, M. H. W. B., & Smilde, A. K. (2020). Corruption of the Pearson correlation coefficient by measurement error and its estimation, bias, and correction under different error models. *Scientific Reports*, *10*(1), 438. https://doi.org/10.1038/s41598-019-57247-4

Scambos, T. A., Bell, R. E., Alley, R. B., Anandakrishnan, S., Bromwich, D. H., Brunt, K., et al. (2017). How much, how fast?: A science review and outlook for research on the instability of Antarctica's Thwaites Glacier in the 21st century. *Global and Planetary Change*, *153*, 16–34. https://doi.org/10.1016/j.gloplacha.2017.04.008

Schober, P., Boer, C., & Schwarte, L. A. (2018). Correlation coefficients: Appropriate use and interpretation. *Anesthesia & Analgesia*, *126*(5), 1763–1768. https://doi.org/10.1213/ane.0000000000002864

Schoof, C. (2006). A variational approach to ice-stream flow. *Journal of Fluid Mechanics*, *556*, 227–251. https://doi.org/10.1017/s0022112006009591

Schroeder, D. M., Blankenship, D. D., & Young, D. A. (2013). Evidence for a water system transition beneath Thwaites Glacier, West Antarctica. *Proceedings of the National Academy of Sciences of the United States of America*, *110*(30), 12225–12228. https://doi.org/10.1073/pnas.1302828110

Schroeder, D. M., Seroussi, H., Chu, W., & Young, D. A. (2016). Adaptively constraining radar attenuation and temperature across the Thwaites Glacier catchment using bed echoes. *Journal of Glaciology*, *62*(236), 1075–1082. https://doi.org/10.1017/jog.2016.100

Seroussi, H., Nowicki, S., Payne, A. J., Goelzer, H., Lipscomb, W. H., Abe-Ouchi, A., et al. (2020). ISMIP6 Antarctica: A multi-model ensemble of the Antarctic ice sheet evolution over the 21st century. *The Cryosphere*, *14*(9), 3033–3070. https://doi.org/10.5194/tc-14-3033-2020

Spearman, C. (1904). The proof and measurement of association between two things. *American Journal of Psychology*, *15*(1), 72–101. https://doi.org/10.2307/1412159

Tsai, C.-Y., Forest, C. E., & Pollard, D. (2017). Assessing the contribution of internal climate variability to anthropogenic changes in ice sheet volume. *Geophysical Research Letters*, *44*(12), 6261–6268. https://doi.org/10.1002/2017GL073443

Tsai, V. C., Stewart, A. L., & Thompson, A. F. (2015). Marine ice-sheet profiles and stability under Coulomb basal conditions. *Journal of Glaciology*, *61*(226), 205–215. https://doi.org/10.3189/2015JoG14J221

Wackerly, D. D., Mendenhall, W., III., & Scheaffer, R. L. (2008). Multivariate probability distributions. In *Mathematical statistics with applications* (7th ed.). Brooks/Cole223–295.

Weertman, J. (1957). On the sliding of glaciers. *Journal of Glaciology*, *3*(21), 33–38. https://doi.org/10.3189/s0022143000024709

Zoet, L. K., & Iverson, N. R. (2020). A slip law for glaciers on deformable beds. *Science*, *368*(6486), 76–78. https://doi.org/10.1126/science.aaz1183